Combustion and Flame 156 (2009) 771–779

Contents lists available at ScienceDirect

Combustion and Flame

www.elsevier.com/locate/combustflame

Effect of cylindrical confinement on the determination of laminar flame speeds using outwardly propagating flames

Michael P. Burke, Zheng Chen, Yiguang Ju*, Frederick L. Dryer

Department of Mechanical and Aerospace Engineering, Princeton University, Princeton, NJ 08544, USA

ARTICLE INFO

Article history:
Received 23 January 2008
Received in revised form 4 January 2009
Accepted 24 January 2009
Available online 25 February 2009

Keywords:
Laminar flame speed
Markstein length
Burning velocity
Outwardly propagating flame
Cylindrical confinement
Cylindrical chamber
Flow correction
Hydrogen
Syngas
High pressure

ABSTRACT

The effect of nonspherical (i.e. cylindrical) bomb geometry on the evolution of outwardly propagating flames and the determination of laminar flame speeds using the conventional constant-pressure technique is investigated experimentally and theoretically. The cylindrical chamber boundary modifies the propagation rate through the interaction of the wall with the flow induced by thermal expansion across the flame (even with constant pressure), which leads to significant distortion of the flame surface for large flame radii. These departures from the unconfined case, especially the resulting nonzero burned gas velocities, can lead to significant errors in flame speeds calculated using the conventional assumptions, especially for large flame radii. For example, at a flame radius of 0.5 times the wall radius, the flame speed calculated neglecting confinement effects can be low by ~15% (even with constant pressure).

A methodology to estimate the effect of nonzero burned gas velocities on the measured flame speed in cylindrical chambers is presented. Modeling and experiments indicate that the effect of confinement can be neglected for flame radii less than 0.3 times the wall radius while still achieving acceptable accuracy (within 3%). The methodology is applied to correct the flame speed for nonzero burned gas speeds, in order to extend the range of flame radii useful for flame speed measurements. Under the proposed scaling, the burned gas speed can be well approximated as a function of only flame radius for a given chamber geometry – i.e. the correction function need only be determined once for an apparatus and then it can be used for any mixture. Results indicate that the flow correction can be used to extract flame speeds for flame radii up to 0.5 times the wall radius with somewhat larger, yet still acceptable uncertainties for the cases studied. Flow-corrected burning velocities are measured for hydrogen and syngas mixtures at atmospheric and elevated pressures. Flow-corrected flame speeds in the small cylindrical chamber used here agree well with previously reported flame speeds from large spherical chambers. Previous papers presenting burning velocities from cylindrical chambers report performing data analysis on flame radii less than 0.5 or 0.6 times the wall radius, where the flame speed calculated neglecting confinement effects may be low by ~15 or 20%, respectively. For cylindrical chambers, data analysis should be restricted to flame radii less than 0.3 times the wall radius or a flow correction should be employed to account for the burned gas motions.

With regard to the design of future vessels, larger vessels that minimize the flow aberrations for the same flame radius are preferred. Larger vessels maximize the relatively unaffected region of data allowing for a more straightforward approach to interpret the experimental data.

1. Introduction

The standard laminar burning velocity of a combustible mixture is defined as the speed at which a one-dimensional (1-D) planar, adiabatic deflagration wave travels through a flammable, quiescent, unburned gas mixture. It is a fundamental parameter of a fuel–oxidizer mixture that governs practical combustion phenomena such as burning rate, blowoff, and flashback. Since all realistic flames are curved and/or travel through a strained flow field, another fundamental mixture parameter known as the Markstein length (defined below), which quantifies the response of the flame speed to strain rate, is also necessary to characterize flame behavior more completely. These two fundamental mixture parameters, the laminar burning velocity and Markstein length, are necessary inputs for flamelet calculations and important validation checkpoints in the development of chemical kinetic and transport models.

Recently, the most common approaches for measuring burning velocity and Markstein length have been the stagnation or counterflow flame method [1–3] and the constant-pressure outwardly

* Corresponding author. Fax: +1 (609) 258 6109.
E-mail addresses: mpburke@princeton.edu (M.P. Burke), zhengc@princeton.edu (Z. Chen), yju@princeton.edu (Y. Ju), fldryer@princeton.edu (F.L. Dryer).

0010-2180/$ – see front matter
doi:10.1016/j.combustflame.2009.01.013

Nomenclature

A_f	infinitesimal flame surface area element
L_u	unburned Markstein length
$\underline{r}$	position vector (cylindrical coordinates, with components r, θ, and z)
r_f	flame distance along r-axis from center
r_w	radius of cylindrical chamber
$R_{w,sph}$	radius of spherical chamber
s_u	stretched unburned flame speed
s_u^o	unstretched laminar burning velocity
$\underline{u}_b$	burned gas velocity vector
$\underline{V}_f$	flame front propagation velocity vector
z_f	flame distance along z-axis from center
z_w	half-length of cylindrical chamber
Greek symbols	
κ	stretch rate
σ	expansion factor
$\underline{\varpi}$	scaled burned gas velocity vector
Subscripts	
r	radial component (cylindrical coordinates)
unc	uncorrected values (based on unconfined assumption)
z	axial component (cylindrical coordinates)

propagating spherical flame method [4–8]. The well defined stretch rates of these flame geometries allow for extrapolation of measured local flame speeds to their fundamental, unstretched values and Markstein lengths [9]. Recently, new techniques have been developed to extend the outwardly propagating flame method to achieve measurements at pressures significantly higher than those used previously [4,5]. While measurements have previously been limited to pressures less than 10 atm, these techniques have allowed for stretch-corrected burning velocity determination up to 60 atm using spherical flames [6].

The constant-pressure spherical flame method involves capturing Schlieren images of an expanding spherical flame and calculating the instantaneous flame speed and stretch from radius–time data [7,8]. Most studies employ the relations given by Strehlow and Savage [10] for an unconfined outwardly propagating spherical flame, in which the burned gas is assumed to come to rest after crossing the flame and the flame is taken to be infinitesimally thin:

$$s_{u,unc} = \frac{1}{\sigma}\frac{dR_f}{dt}, \tag{1}$$

$$\kappa_{unc} = \frac{2}{R_f}\frac{dR_f}{dt}. \tag{2}$$

Here $s_{u,unc}$ is the uncorrected stretched flame speed, κ_{unc} the uncorrected stretch rate, R_f the spherical flame radius, and dR_f/dt the flame propagation speed, V_f. The thermal expansion factor, σ, is defined as the ratio of unburned to burned gas density. Equations (1) and (2) will henceforth be referred to as the unconfined relations. There are various methods found in the literature for relating stretch rate and stretched flame speed such that the fundamental mixture parameters, the unstretched laminar burning velocity, s_u^o, and Markstein length, L_u, can be extracted as described in Refs. [7,11–14]. The present study uses a commonly employed relation, first postulated by Markstein [11]:

$$s_u = s_u^o - L_u \cdot \kappa. \tag{3}$$

Equation (3) was derived from asymptotic theory for weakly stretched flames [15] and has been found to hold for more general conditions, as discussed in Ref. [16]. The unstretched laminar burning velocity and the Markstein length can be extracted from experimental data through a linear regression analysis (Eq. (3)).

For the aforementioned spherical-flame theory to be satisfied exactly, it requires an unwrinkled, spherical, infinitesimally thin, weakly stretched, adiabatic, quasi-steady flame with a constant expansion factor in a zero-gravity, unconfined environment. These assumptions are not satisfied in practical cases and, consequently, numerous studies have been devoted to quantification and correction of the errors incurred by departures from the theoretical assumptions. The departures that have been investigated include finite flame thickness [17], ignition disturbances [13,18], pressure rise in spherical confinement [19–26], compression-induced burned gas velocities in spherical confinement [26], varying density ratio [12], radiation [12,27], gravity [28,29], flame front wrinkling [30–33], nonlinear behavior [34], and unsteady behavior and flame speed reverse [35]. While Sivashinsky performed a theoretical analysis of an outwardly propagating flame in an arbitrary confinement [36], the majority of studies on confinement effects focused on spherical chambers [19–26].

However, in order to achieve flame speed measurements at high pressures, many of the outwardly propagating flame experiments have been conducted in cylindrical [4,5,25,37–39] or cuboid-shaped [40] chambers. Many of the facilities designed for pressures above 10 atm with optical access (necessary for the constant-pressure method) are cylindrical [4,5,25,37–39]. Frequently, these high-pressure, nonspherical chambers are often smaller than typical spherical bombs (for safety reasons) such that flame speeds are measured for flames closer to the chamber walls. Therefore, determination of the effect of nonspherical confinement is necessary to assess the validity of the assumptions commonly employed for laminar flame speed measurement as well as to improve the accuracy of these measurements. While a previous study mentioned the possibility of "wall interference" in these cylindrical bombs at large radii [6], the mechanism through which the wall interferes with the flame evolution has not been investigated in detail for cylindrical chambers. The extent to which this interference affects flame speed measurement has also not been quantified previously. As we discuss below, the cylindrical chamber geometry disrupts the induced flow field from the unconfined case, causing significant departures from the commonly employed theory and leading to substantial errors in flame speed measurement at large flame radius relative to the wall radius, even for constant chamber pressure.

The present study explores the effects of cylindrical-geometry confinement on outwardly propagating flames and the determination of laminar flame speed. The primary focus is on the manifestation of this effect in the flame shape evolution, flame propagation speed, and burned gas speeds along the r-axis in chambers having a length greater than their diameter. These factors and conditions encompass all of the research conducted previously in cylindrical chambers [4,5,25,37–39].

2. Experimental methods

2.1. Description

Experiments were conducted in a dual-chambered, pressure-release type high-pressure combustion apparatus shown in Fig. 1. Complete details of the experimental apparatus and procedure can

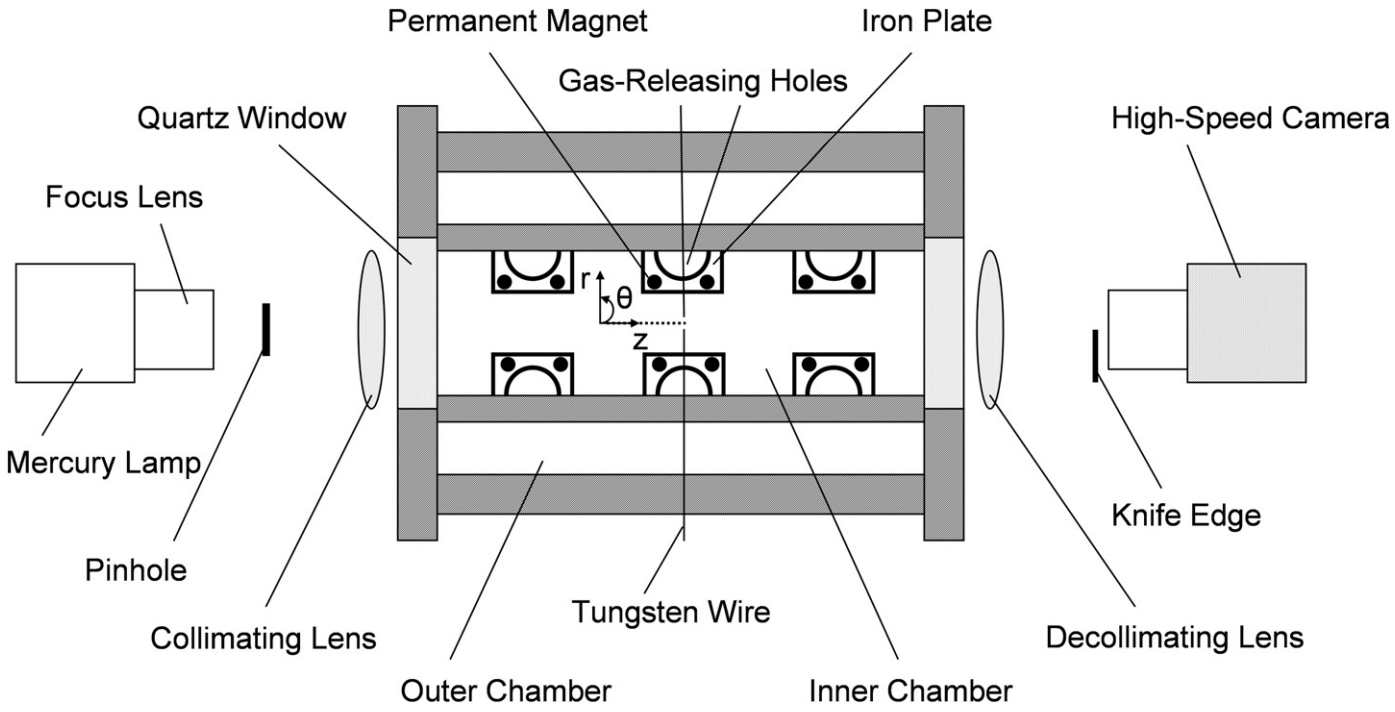

Fig. 1. Diagram of the experimental apparatus.

be found in Ref. [5]. The chamber consists of two concentric cylindrical vessels of inner diameters 10 and 28 cm. The length of the inner chamber is 15.24 cm. Twelve circular holes of 2.2 cm diameter are located in the radial wall of the inner vessel at z-offsets of -4.6, 0, and 4.6 cm and θ-offsets of 45, 135, 225 and 315 degrees to allow for pressure release. These holes can be sealed with O-rings under the compression of iron plates attracted by a series of permanent magnets embedded in the wall. The iron plates provide a seal between chambers for pressure differences between outer and inner chambers greater than 0.3 atm. When the pressure difference vanishes or reverses, the iron plates dislodge, allowing gases to flow from the inner to the outer chamber to maintain a nearly constant pressure. Since the inner vessel volume is 10 times smaller than that of the outer, the total pressure increase after combustion is small, ensuring not only a nearly constant-pressure experiment, but operational safety for experiments conducted at high initial unburned gas pressures. For the present experiments, however, the magnetic plates were either removed entirely, or remained in place (holes sealed) throughout each experiment to avoid transitions in flow field boundary conditions. The two configurations described will hereafter be called "open" chamber and "closed" chamber experiments, respectively. It should be noted that the inner cylindrical wall has cavities leading to the magnetic plates as well as gas inlet and outlet holes. Thus, some aberration in the flame evolution from the perfectly cylindrical case is expected to be present at large flame radii (as the flame structure approaches the side wall holes).

Mixtures were prepared using the partial pressure method with hydrogen (99.99%), nitrogen (99.998%), oxygen (99.5%), and carbon monoxide (99.99%) stored in an aluminum cylinder. Schlieren photography was utilized for imaging the flame propagation. Light from a 100 W mercury lamp is focused on a 100 μm pinhole and collimated by a spherical lens. The collimated light passes through windows to the inner chamber and is focused on a horizontally installed knife edge. A high-speed digital video camera with 4 μs shutter speed and frame rates of 8000 to 24,000 fps is used to record images of the propagating flame. The flame front is located from these images and the flame radius along $\theta = 0°$, r_f, is obtained using an automated detection program for ease of processing and reduction of human bias. The raw r_f data are smoothed and radial propagation speed, $V_{f,r}$, is calculated using local, least-squares second order polynomial fitting methods for data within 3 mm of the radius of interest. Data processed in this manner are consistent with the raw data as well as data processed through a more conventional local-averaging (low-pass) filter.

2.2. Discussion of uncertainties

Any of the various departures mentioned in Section 1 for relating V_f to s_u and s_u to s_u^o as well as uncertainties in the measurement of V_f contribute to the uncertainty in s_u and s_u^o determined from experiment. Here, we focus on uncertainties and errors associated with the effect of confinement and those introduced by the flow correction methodology discussed in Section 4.2. In the figures below, we present error bars for flow-corrected burning velocities calculated from (a) the RMS sum of the observed scatter in our data (±3%, see Fig. 4); (b) uncertainty in assuming the scaled burned gas speed, ϖ_r, to be the same for every mixture (as defined in (4) and discussed in Section 4.1 below); (c) the uncertainty in the extrapolation to zero stretch resulting from a change in the flame speed caused by pressure and temperature rise in the chamber as a function of flame radius. Based on the discussion for Fig. 6, we evaluate the uncertainty in assuming the same scaled burned gas speed for every mixture as 1% for $r_f < 0.3r_w$ and 2% for $r_f < 0.5r_w$. The pressure and temperature rise are approximated based on equations for flame propagation in a spherical chamber using the equivalent wall radius, $R_{w,eff} = (3V/4\pi)^{1/3}$, from [26] where V is the volume of the chamber. The sensitivity to pressure rise and sensitivity to temperature rise were calculated using the mechanism of Li et al. [41]. The uncertainty in the uncorrected burning velocity includes the uncertainties mentioned above in addition to errors due to neglecting the burned gas speed.

3. Modeling

3.1. Description

A simple model for flame propagation was used to qualitatively and quantitatively describe the effect of flow field asymmetries on the evolution of an initially spherical flame in the early stages of propagation, where the effect of confinement is nontrivial but weak. In a manner similar to front-tracking methods described in [42,43], the flame is described by a flamelet model and the flow field is treated as incompressible with a distributed source term for thermal expansion at the flame front and a uniform sink term for compression of the fluid. The flow is further approximated as irrotational (which is reasonable for small r_f, but cannot be ignored for large r_f as discussed below). A weakly stretched flamelet model, i.e. Eq. (3), is used with κ, the local instantaneous stretch rate, defined as $d\ln(A_f)/dt$, with A_f being the area of an infinitesimal flame surface element. The boundary conditions for the closed cylindrical chamber used were inviscid walls. The initial condition is a spherical flame of flame radius of $0.1r_w$, with the stretch rate and flame speed of an unconfined flame given by Eqs. (1) and (2). The numerical results are smoothed using a locally weighted scatter smoothing (i.e. LOWESS) scheme [44] to remove oscillations introduced by the numerical scheme.

The flamelet model requires input values for s_u^o, L_u, and σ. Here s_u^o, L_u, and σ are chosen to represent experimental mixtures (as in Figs. 2–4). Values for s_u^o and L_u were calculated from the experimental data through a linear regression of Eq. (3) using the flow-corrected flame speed presented in the next section. Expansion factors, σ, were obtained from planar flame calculations [45] using the thermochemical parameters of Li et al. [41].

The model used here is similar to Sivashinsky's model [36] in the limiting case where the pressure rise in the chamber is small except that the effect of stretch on flame speed is included here by adopting Eq. (3) as the more relevant flamelet model. This flame speed relation is chosen in lieu of one relating flame speed to pressure and temperature rise as used in [36] since we are interested in the early stages where stretch effects are far greater than pressure effects (and in fact the direct pressure effect on the flame speed can be reasonably neglected when the ratio of burned gas volume to the chamber volume is less than 0.125 [26]).

3.2. Limitations of the model

The accuracy of the model is expected to be questionable when the flame is close enough to the wall such that (1) the distorted flame shape and flow field produce appreciable levels of flame generated vorticity and/or (2) the upstream temperature and pressure rise caused by isentropic compression result in a change in density ratio, planar burning velocity and Markstein length.

Estimates of flame generated vorticity were made based on the tangential pressure gradient calculated in the simulations. The results indicate that the baroclinic torque produced by a flame in a cylindrical chamber is the same order of magnitude or less than baroclinic torque produced by gravity for an unconfined flame (for a stoichiometric H_2–air mixture for $r_f < 0.5r_w$). Since baroclinic torque produced by gravity is generally considered small for outwardly propagating flames, rotational effects are not expected to be significant for the flames with relatively small values of r_f/r_w of interest here.

Results from the simulations indicated that the relative pressure rise for $r_f = 0.5r_w$ was less than about 7%, leading to a temperature rise of less than about 2% for all relevant mixtures in a chamber of aspect ratio 1.5. For a stoichiometric H_2–air mixture, for example, this corresponds to a change in the burned flame speed of less than 1% at $r_f = 0.5r_w$. Since the pressure and temperature rise due to compression in the chamber are not included in the model or the flow correction methodology, the response of the flame speed to pressure and temperature rise contribute to the uncertainty in the results.

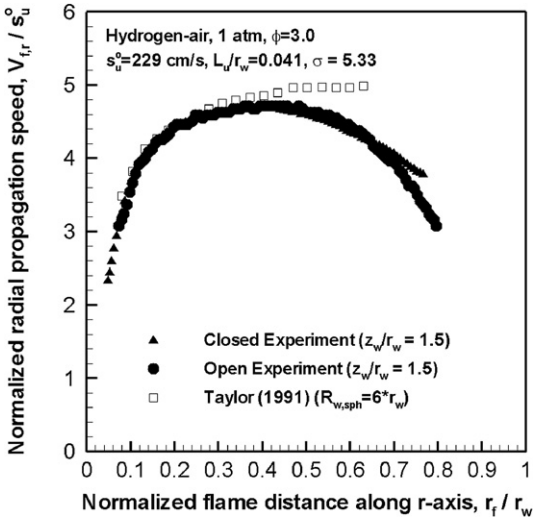

Fig. 2. Normalized flame propagation speed in the radial direction for experiments with open or closed test chamber (see text) compared to previous measurements in large spherical bomb [12].

As demonstrated in Section 4.1, the fluid-mechanical model used here demonstrates significant improvements over the unconfined model, which is typically applied to flame speed determination in cylindrical chambers. The model is validated against data from a wide range of flame conditions in Section 4 below. Moreover, numerical solutions of this reduced model offer significant advantages in terms of computational time over detailed, multidimensional, unsteady simulations, thus allowing for parametric studies to be performed.

4. Results and discussion

4.1. Flame evolution in cylindrical confinement

The experimental data for flame propagation speed history in the radial direction for the closed and open cases (as described in Section 2) are presented in Fig. 2 for an equivalence ratio of 3.0. Flame speed data obtained in a large spherical chamber ($R_{w,sph} = 30\text{ cm} = 6r_w$) from [12] are also plotted for comparison. For such a large chamber, the compression effect is small for $r_f < 5$ cm and the expanding flame behaves as if it were unconfined. The data from the cylindrical chamber show an initial increase in radial propagation speed followed by a decrease with increasing r_f, whereas the data from Taylor from the larger chamber continue to increase with r_f. The initial increase in propagation speed can be attributed to the effect of decreasing stretch on flame speed for a mixture with a positive Markstein length. The decrease in radial propagation speed in the cylindrical bomb can be attributed to the effect of confinement distorting the flow field. The confinement effect is observed for both constant-volume and constant-pressure experiments. Therefore, pressure rise is not necessary for the confinement to affect the flame propagation in nonspherical chambers (as would be the case for spherical chambers).

For $r_f < 0.3r_w$, the flame propagation speed measured in the cylindrical bomb agrees well with that measured in a larger spherical vessel. However, for $r_f > 0.3r_w$, the difference between the propagation speeds in the cylindrical chamber and the larger

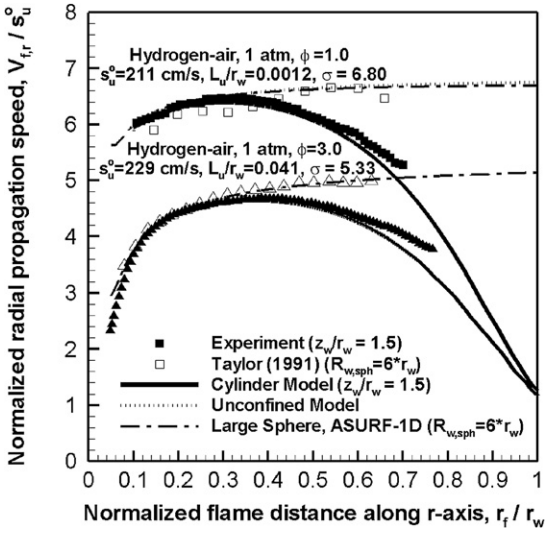

Fig. 3. Normalized flame propagation speed in the radial direction: comparison of experimental traces with model results for flames in a small cylindrical chamber, and experimental [12] and numerical results for flames in a large spherical chamber.

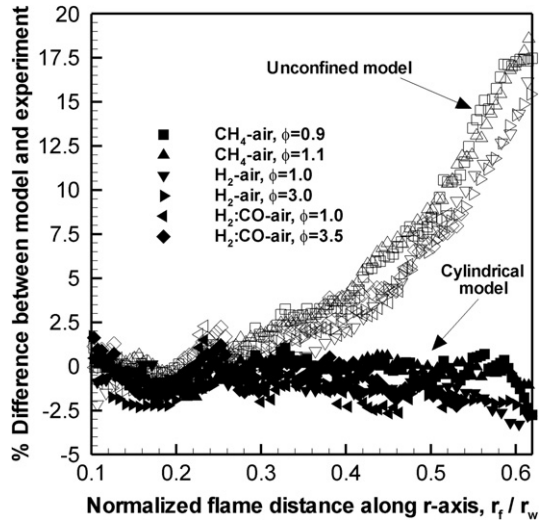

Fig. 4. Percent difference between models and experiment for a variety of mixtures.

spherical chamber becomes larger than the ~3% degree of scatter observed in the data (see Fig. 4).

Fig. 3 presents the experimental data for flame propagation speed history along the r-axis of a closed cylindrical chamber for equivalence ratios of 1.0 and 3.0 and the numerical solution of the flamelet model for a cylindrical chamber of the same aspect ratio as the experiment. These results are contrasted with flame speed data obtained in a large spherical chamber ($R_{w,sph} = 30\ \text{cm} = 6r_w$) from [12], simulations for a spherical chamber of the same size ($R_{w,sph} = 30\ \text{cm} = 6r_w$) using direct numerical simulation (in-house code, ASURF-1D, described in detail and validated in [26]), and calculations based on the unconfined flame relations, (1) and (2).

The experimental data and the model solution for the cylindrical chamber are nearly identical to the unconfined model as well as experimental data and A-SURF-1D predictions for the large spherical chamber, during the early stages of propagation ($r_f < 0.3r_w$). For these conditions, the flow field is relatively unaffected by the cylindrical boundary. The radial flame propagation speed initially increases with r_f due to an increase in the unburned flame speed with decreasing stretch and a positive Markstein length. As the flame progresses to larger values of r_f, however, the radial flame propagation speed in the cylindrical chamber becomes lower than the unconfined case because the flow is compressed in the radial direction.

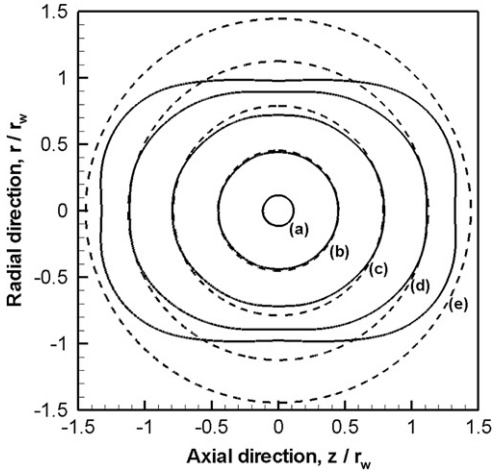

Fig. 5. Comparison of flame surface contours for a flame in a finite-length cylindrical chamber of aspect ratio, $z_w/r_w = 1.5$, and an unconfined flame for $\sigma = 8$ at (a) 0.002, (b) 0.044, (c) 0.086, (d) 0.128, (e) 0.170 r_w/s_u^0.

The cylindrical model solution demonstrates excellent agreement with experimental data from the cylindrical chamber – within ~3% for $r_f < 0.6r_w$. However, agreement between the model results and experimental data degrades for $r_f > 0.6r_w$ due to the aforementioned limitations in the model and the experimental effects of the cavities in the chamber wall. The difference between experimental data and model predictions using the conventional unconfined model and the present cylindrical model are compared in Fig. 4 for hydrogen–air, syngas–air, and methane–air mixtures of various equivalence ratios. The cylindrical model provides significant improvements over the unconfined model at larger r_f. While the unconfined model over-predicts the propagation speed by nearly 20%, the cylindrical model predicts the experimentally measured propagation speed within the data scatter for $r_f < 0.6r_w$.

Since the r–z plane (where the flame surface distortion is evident) is not optically accessible in the experimental apparatus used, the flamelet model is used to study the evolution of the flame surface in a cylindrical chamber. Fig. 5 shows the r–z plane cross-sections of the flame surface compared to that of an unconfined flame with $\sigma = 8$ and $L_u/r_w = 0$ at successive times. During the early stages, corresponding to the stage labeled (a) in Fig. 5, the gas velocity is zero everywhere in the burned gas zone, and the flame shape remains the same as that of the unconfined flame. However, as the flame progresses, i.e. (b) and (c) in Fig. 5, the burned gas speed becomes negative along the r-axis and positive along the z-axis. These burned gas speeds result in a reduced propagation rate along the r-axis and enhanced propagation rate along the z-axis. The difference in propagation rates produces a distorted flame surface at stages (c), (d), and (e) – compressed in the radial direction and stretched in the axial direction, compared to the unconfined case. The acceleration of the flame front in the z-direction is minor for the present aspect ratio, but for higher aspect ratios, the acceleration will be more pronounced. We have reported observations of distorted flame fronts that were visualized in a cuboid-shaped chamber in our previous work [46], which provides clear experimental evidence of the deformation of the flame surface due to nonspherical confinement.

The modified evolution in cylindrical confinement is caused by the nonzero burned gas velocities imposed by the walls. Since the burned gas speed is initially zero and increases to $(\sigma - 1)s_u$ when

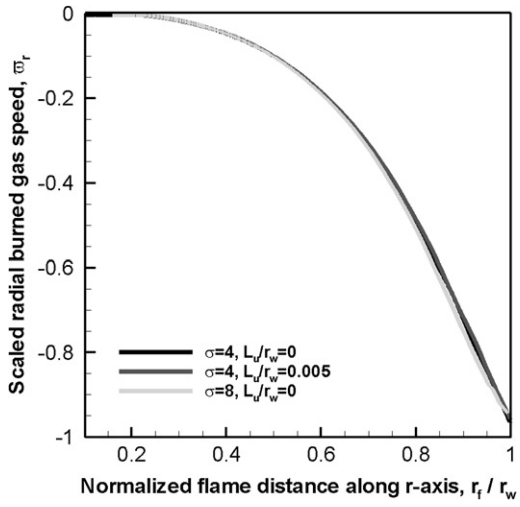

Fig. 6. Scaled burned gas speed in the radial direction for various mixture parameters for $z_w/r_w = 1.5$.

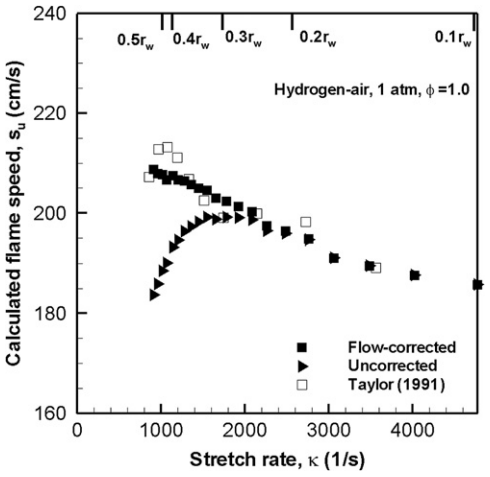

Fig. 7. Calculated flame speed for a hydrogen–air mixture of equivalence ratio of 1.0 at 1 atm obtained in a cylindrical chamber ($r_w = 5$ cm, $z_w/r_w = 1.5$) with and without flow correction compared to calculated flame speed obtained in a large spherical chamber [12] ($R_w = 30$ cm) as a function of stretch.

the flame reaches the wall, we define a scaled burned gas velocity as

$$\varpi = \frac{u_b}{(\sigma - 1)s_u} \tag{4}$$

in order to generalize the flow field response to the confinement for different mixtures. The scaled burned gas speed along the r-axis, ϖ_r, obtained from the model results is plotted as a function of r_f/r_w for different mixture parameters in Fig. 6. The mixture parameters shown in Fig. 6 were chosen to cover a reasonable range of typical mixture conditions. Though the burned gas speeds as a function of r_f/r_w for the different cases are very different, the scaled burned gas speeds for all the mixtures collapse onto a single curve. The scaled burned gas speeds for the three cases are within 1% for $r_f < 0.4r_w$ and 3% for $r_f < 0.6r_w$, and the burned gas speeds have nearly the same profile for chambers of different aspect ratios (not shown here due to space considerations). In fact, for aspect ratios of 1.5 or larger, the differences among the burned gas speeds are less than 5% for $r_f < 0.6r_w$. The effect of cylindrical confinement on the flame propagation speed and burned gas speed is slightly stronger for larger aspect ratios.

4.2. Effect of cylindrical confinement on laminar flame speed measurement and an algorithm for flow correction

Cylindrical confinement limits the applicability of the conventional (uncorrected) constant-pressure method for flame speed calculations in two ways: (1) a disruption of spherical symmetry and (2) nonzero velocities in the burned gas zone. In the modeling results, the stretch rate was found to closely follow the spherical prediction, indicating that Eq. (2) can still be used to calculate the stretch rate using r_f and dr_f/dt from the experiments. In fact, the stretch rate calculated using the definition of stretch as $d\ln(A_f)/dt$ and the stretch rate using (2), differ by less than 5% for $r_f < 0.6r_w$, resulting in negligible differences in extrapolated burning velocity and Markstein length. Therefore, for sake of simplicity in applying the correction methodology, Eq. (2) can be used to approximate the stretch rate without incurring appreciable errors. However, the results from the last section indicate that the zero burned gas velocity assumption commonly employed in constant-pressure flame speed calculations can be strongly violated in cylindrical chambers even when the pressure in the chamber is nearly constant. The radial propagation speed, $V_{f,r}$, can be related to the flame speed and radial burned gas speed, $u_{b,r}$, through

$$V_{r,f} = \sigma \cdot s_u + u_{b,r}. \tag{5}$$

Combining Eqs. (1), (4), and (5) in the radial direction yields

$$\frac{s_{u,unc} - s_u}{s_u} = \frac{\sigma - 1}{\sigma}\varpi_r. \tag{6}$$

Equation (6) is a measure of the error in using the unconfined (uncorrected) relations for a given scaled burned gas speed. In Eq. (6) $s_{u,unc}$ is the stretched flame speed calculated assuming no confinement, Eq. (1), and is, therefore, the "uncorrected" flame speed. Since the scaled burned gas speed along the r-axis, ϖ_r, has been shown to be well-approximated as a function of only r_f/r_w and is of order unity, Eq. (6) shows that the error in the unconfined assumption is proportional to $(\sigma - 1)/\sigma$.

Since the confinement effect is stronger when the flame is closer to the wall, extrapolating to obtain the planar burning velocity and Markstein length using Eq. (3), assuming zero burned gas velocity over ranges of large r_f/r_w will yield erroneous results, as demonstrated in Fig. 7. For large stretch rates (small r_f/r_w), the calculated flame speed using (1) is consistent with flame speed data taken in a large spherical bomb [12]. Then, as the stretch rate decreases (r_f/r_w increases), the flame speed calculated using the zero burned gas velocity assumption decreases significantly due to the effect of confinement.

A flow-corrected flame speed, which accounts for the actual induced fluid motions in the confinement, can be calculated by a rearrangement of Eq. (6) using Eq. (1)

$$s_u = \frac{V_{f,r}/\sigma}{\left(1 + \frac{\sigma-1}{\sigma}\varpi_r\right)}. \tag{7}$$

Since the scaled radial burned gas speed, ϖ_r, is well-approximated as a function of r_f/r_w only (independent of mixture properties), the same correction can be used for every experiment for a given cylindrical chamber. Thus, the flow correction need only be determined once, and then the results can be used for all mixtures.

The flow-corrected flame speed, calculated using the scaled radial burned gas speed obtained from the modeling results in Eq. (7), is also presented in Fig. 7. The flow-corrected flame speed is shown to follow closely the flame speed data obtained in a larger spherical bomb by Taylor [12] (shown in Fig. 7) – as well as other data from large bombs [47,48] – over a much wider span of stretch rates than the uncorrected flame speed. The values of the uncorrected data are much lower than those of the flow-corrected data from the cylindrical bomb and flame speed data from large spherical bombs at large r_f/r_w. As demonstrated in Fig. 10 below, failure to account for the induced fluid motions yields large errors

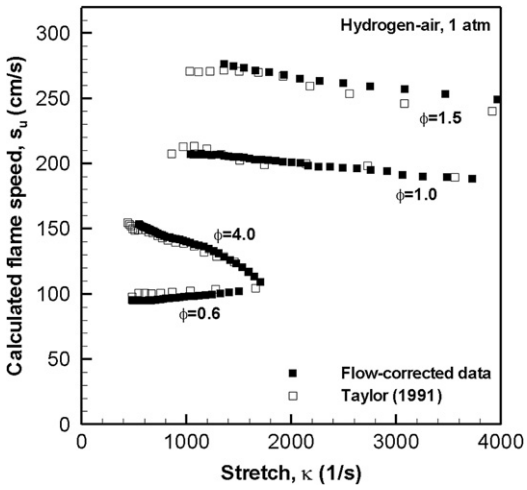

Fig. 8. Comparison of flow-corrected flame speeds obtained in a cylindrical chamber ($r_w = 5$ cm, $z_w/r_w = 1.5$) with flame speeds obtained from a larger bomb [12] ($R_w = 30$ cm) as a function of stretch.

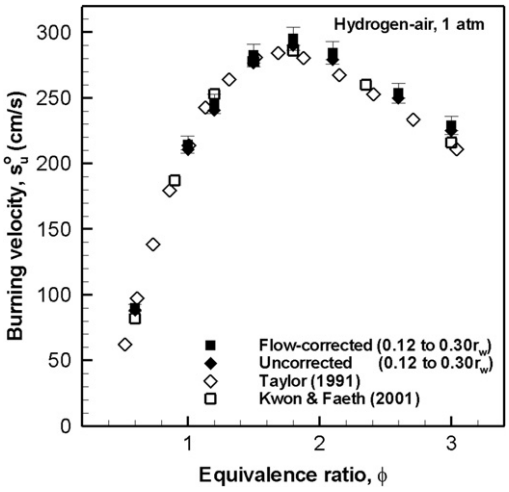

Fig. 9. Comparison of flow-corrected and uncorrected burning velocities extrapolated over $0.12r_w < r_f < 0.3r_w$ and burning velocities from larger bombs [12,49] for hydrogen–air mixtures. (For $r_f < 0.3r_w$, the flame is relatively unaffected by the confinement.)

in extrapolation of planar burning velocity (as well as Markstein length) if data of large r_f/r_w are used.

Similar results are obtained for a wide range of equivalence ratios of hydrogen, syngas, and methane mixtures which have different values for the flame speed, Markstein length, and expansion factor.

4.3. Demonstration of methodology – flow corrected flame speeds for hydrogen and syngas mixtures

Flow-corrected flame speeds as a function of stretch obtained in our cylindrical chamber are compared with flame speeds obtained in a large spherical chamber [12] for hydrogen–air mixtures of equivalence ratios from 0.6 to 4.0 in Fig. 8. The flow-corrected flame speeds agree well with the large bomb measurements over the whole range of stretch rate spanned for $r_f < 0.5r_w$. Similar agreement is observed for methane–air mixtures.

Fig. 9 shows flow-corrected and uncorrected burning velocities extrapolated over the range $0.12r_w < r_f < 0.3r_w$ along with burning velocities obtained in larger bombs. The burning velocities obtained from our cylindrical bomb agree well with other published burning velocities. The flow-corrected and uncorrected

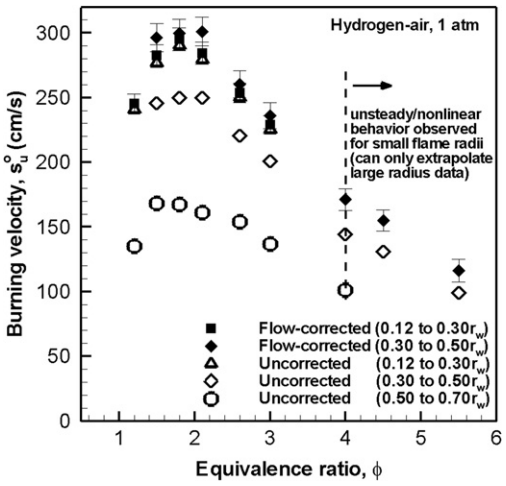

Fig. 10. Effect of data range on extrapolated burning velocity for hydrogen–air mixtures.

burning velocities for this extrapolation range agree within ~3% – corroborating the results presented above, which imply that flames of $r_f < 0.3r_w$, are relatively unaffected by the confinement effect.

The flow-corrected and uncorrected burning velocities obtained from extrapolations over different data ranges are plotted in Fig. 10. Ranges over large r_f are excluded if wrinkling is observed and ranges over small r_f are excluded if nonlinear or unsteady effects are noted. For equivalence ratios where both extrapolation ranges are unaffected by wrinkling, nonlinear or unsteady behavior, the flow-corrected burning velocities obtained using two different data ranges agree within ~5%. Flow-corrected burning velocities for the range from $0.3r_w < r_f < 0.5r_w$ have somewhat larger uncertainties than those for $0.12r_w < r_f < 0.3r_w$. The uncertainty due to pressure and temperature rise in the chamber is estimated to be 4% or below for equivalence ratios less than 4.5 and 7% for an equivalence ratio of 5.5. However, uncorrected burning velocities extrapolated over $0.3r_w < r_f < 0.5r_w$ and $0.5r_w < r_f < 0.7r_w$ are consistently lower than the flow-corrected and uncorrected burning velocities extrapolated over $0.12r_w < r_f < 0.3r_w$ by ~15% and ~40%, respectively.

For equivalence ratios of 4.0 and larger, nonlinear and unsteady effects were observed in flames during the range $0.12r_w < r_f < 0.3r_w$. Under these circumstances, only large radius ranges can be used for linear extrapolation. A flow correction can be employed to extend the range that can be used for extrapolation, thus allowing for determinations of burning velocity for these mixtures with somewhat larger uncertainties. The methodology provides a significant improvement over neglecting the burned gas velocity, which results in a ~15% error, for this range from $0.3r_w < r_f < 0.5r_w$. Similar results are obtained for a variety of fuels and pressures.

For example, Fig. 11 presents flow-corrected burning velocities for syngas mixtures at various pressures. For the atmospheric pressure cases, an H_2:CO = 50:50 syngas mixture in air was studied. For the elevated pressure cases, an H_2:CO = 25:75 syngas mixture in $O_2 + 7$He oxidizer was studied. The range used for extrapolation was $0.12r_w < r_f < 0.3r_w$, except for equivalence ratios 1.6 and 2.0 at 20 atm where $0.12r_w < r_f < 0.22r_w$ is used (since the flame is wrinkled for larger radii). Analogous to the results for atmospheric hydrogen–air, the flow-corrected burning velocities obtained using two different data ranges, $0.12r_w < r_f < 0.3r_w$ and $0.3r_w < r_f < 0.5r_w$, agree within ~5% for equivalence ratios where both extrapolation ranges are unaffected by wrinkling, nonlinear or unsteady behavior. Uncorrected syngas burning velocities using the range $0.3r_w < r_f < 0.5r_w$ are also consistently lower by ~15%.

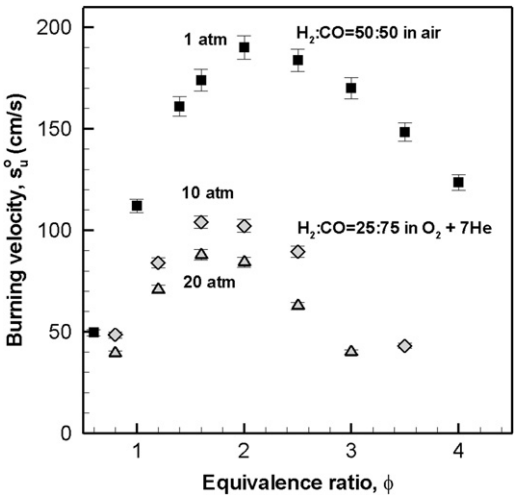

Fig. 11. Syngas burning velocities at atmospheric and high pressures.

4.4. Additional notes

Where possible, it is recommended that the early portion of the data ($r_f < 0.3r_w$) is used in cylindrical bomb experiments. For this part of the data range, the experimental and modeling results indicate that the effect of cylindrical confinement is small. The uncorrected and flow-corrected flame speeds agree within 3% for this range. However, for some mixtures the early region might be strongly influenced by ignition transients [35] or nonlinear behavior [34]. Since these effects are most prominent in mixtures of high Lewis number, one would expect to observe them in lean mixtures of large molecular weight hydrocarbons in addition to rich hydrogen mixtures. For these conditions, a flow correction could be applied to obtain a burning velocity using ranges up to $r_f = 0.5r_w$ with somewhat larger uncertainties. With regard to the design of future vessels, larger vessels that minimize the flow aberrations for the same r_f are preferred since the use of the unaffected data range is a more straightforward approach to interpret the experimental data.

It should be noted that similar flow disturbances caused by the chamber boundaries discussed here occur in all chamber geometries, including spheres, cylinders, and cuboids. Complications arise with "nearly constant-pressure" chambers, as in the present study and Ref. [5], when the pressure-release mechanisms are activated. It is advised that the chamber be kept closed during the stages of the flame development of interest so that the flow field can be described by closed cylindrical chamber flow.

Flow disturbances in nonspherical chambers are likely to pose more significant challenges for the constant-volume flame speeds determined based upon the system pressure history (see any of Refs. [19–25] for a general description). The methodology assumes a spherical flame shape in the calculation of flame area. The pressure rise method emphasizes the late flame evolution process, where the flame shape will be most distorted. Since the conventional expressions employed use a spherical definition for flame area, the distorted flame shape caused by the cylindrical confinement will degrade the accuracy of this definition and will likely yield erroneous results for flame speed.

Previous papers presenting burning velocities from cylindrical chambers report performing data analysis on flame radius ranges of $r_f < 0.5r_w$ or $r_f < 0.6r_w$ [4–6,50]. Substituting values for ϖ_r from Fig. 6 into (6) for typical values of σ implies that the flame speed calculated from (1) is low by ~15% at $r_f = 0.5r_w$ and ~20% at $r_f = 0.6r_w$. Since insufficient details about the chamber geometry, pressure-release timing, and exact range used for extrapolation are available in many of these studies [4–6,50,51], it is unclear if or by how much the burning velocities are affected by confinement effects.

Rate constants for certain reactions, such as radical–radical recombination reactions, which are most important in high pressure flames, have been modified or optimized in several mechanisms [41,51–53] to match high pressure flame speed data from cylindrical chambers. Given the findings of the present study, the high-pressure flame speed measurements utilized in these model validations may require additional scrutiny.

5. Conclusions

The effect of cylindrical confinement on the evolution of outwardly propagating flames and the determination of laminar flame speeds was investigated experimentally and theoretically for chambers having a length greater than their diameter. The major conclusions are:

1. The flame appears to be relatively unaffected by confinement for $r_f < 0.3r_w$. However, for $r_f > 0.3r_w$, the boundary conditions imposed by the confinement induce nonzero burned gas velocities, resulting in a reduction of the radial flame propagation speed from the unconfined case (even for constant pressure). Extrapolation to an unstretched burning velocity using ranges of data for $r_f > 0.3r_w$ yield substantial errors using the unconfined theory, with larger errors incurred at larger r_f.
2. Previous papers presenting burning velocities from cylindrical chambers report performing data analysis on flame radius ranges of $r_f < 0.5r_w$ or $r_f < 0.6r_w$, where the flame speed calculated from (1) may be low by ~15 or 20%, respectively. Since insufficient details about the chamber geometry, pressure-release timing, and exact range used for extrapolation are available in many of these studies, it is unclear if or by how much the burning velocities are affected by confinement effects.
3. A flow correction methodology was developed to account for the nonzero burned gas velocities produced by the cylindrical chamber walls. Under the proposed scaling, the burned gas speed can be well approximated as a function of only r_f for a given chamber geometry – i.e. the correction function need only be determined once for an apparatus and then it can be used for any mixture. The proposed flow correction methodology was demonstrated to allow for flame speed and burning velocity determination for $r_f < 0.5r_w$ with somewhat larger uncertainties. Flow-corrected burning velocities were measured for hydrogen and syngas mixtures at normal and elevated pressures.
4. With regard to the design of future vessels, larger vessels that minimize the flow aberrations for the same r_f are preferred. Larger vessels maximize the relatively unaffected region of data allowing for a more straightforward approach to interpret the experimental data.

Acknowledgments

The research at Princeton University was supported by the U.S. Department of Energy by grant #DE-FG26-06NT42716 and the Petroleum Research Fund from American Chemistry Society by grant PRF#43460-AC5. We wish to thank Dr. Marcos Chaos for assistance in the editing process and Andrew Kelley of Prof. C.K. Law's group at Princeton University for helpful discussions and use of his flame front detection program.

References

[1] Z. Zhao, A. Kazakov, J. Li, F.L. Dryer, Combust. Sci. Technol. 176 (2004) 1–19.
[2] G. Jomaas, X.L. Zheng, D.L. Zhu, C.K. Law, Proc. Combust. Inst. 30 (2004) 193–200.

[3] K. Kumar, C.-J. Sung, Combust. Flame 151 (2007) 209–224.
[4] S.D. Tse, D.L. Zhu, C.K. Law, Proc. Combust. Inst. 28 (2000) 1793–1800.
[5] X. Qin, Y. Ju, Proc. Combust. Inst. 30 (2005) 233–240.
[6] G. Rozenchan, D.L. Zhu, C.K. Law, S.D. Tse, Proc. Combust. Inst. 29 (2002) 1461–1469.
[7] D.R. Dowdy, D.B. Smith, S.C. Taylor, A. Williams, Proc. Combust. Inst. 23 (1990) 325–332.
[8] S. Kwon, L.K. Tseng, G.M. Faeth, Combust. Flame 90 (1992) 230–246.
[9] C.K. Wu, C.K. Law, Proc. Combust. Inst. 20 (1985) 1941–1949.
[10] R.A. Strehlow, L.D. Savage, Combust. Flame 31 (1978) 209–211.
[11] G.H. Markstein, Non-Steady Flame Propagation, Pergamon, New York, 1964, p. 22.
[12] S.C. Taylor, Ph.D. thesis, University of Leeds, Leeds, UK, 1991.
[13] D. Bradley, P.H. Gaskell, X.J. Gu, Combust. Flame 104 (1996) 176–198.
[14] V.F. Karpov, A.N. Lipatnikov, P. Wolanski, Combust. Flame 109 (1996) 436–448.
[15] P. Clavin, Prog. Energy Combust. Sci. 11 (1985) 1–59.
[16] L. Qiao, C.H. Kim, G.M. Faeth, Combust. Flame 143 (2005) 79–96.
[17] L.K. Tseng, M.A. Ismail, G.M. Faeth, Combust. Flame 95 (1993) 410–426.
[18] S.Y. Liao, D.M. Jiang, J. Gao, Z.H. Huang, Q. Cheng, Fuel 83 (2004) 1281–1288.
[19] B. Lewis, G.J. Von Elbe, J. Chem. Phys. 2 (1934) 283–290.
[20] D. Bradley, A. Mitcheson, Combust. Flame 26 (1976) 201–217.
[21] P.G. Hill, J. Huang, Combust. Sci. Technol. 60 (1988) 17–30.
[22] D.A. Daly, J.M. Simmie, J. Würmel, N. Djebaili-Chaumeix, C.E. Paillard, Combust. Flame 125 (2001) 1329–1340.
[23] K. Saeed, C.R. Stone, Combust. Flame 139 (2004) 152–166.
[24] K. Takizawa, A. Takahashi, K. Tokuhashi, S. Kondo, A. Sekiya, Combust. Flame 141 (2005) 298–307.
[25] F. Parsinejad, C. Arcari, H. Metghalchi, Combust. Sci. Technol. 178 (2006) 975–1000.
[26] Z. Chen, M.P. Burke, Y. Ju, Combust. Theory Model. (2009), in press.
[27] I.C. McLean, D.B. Smith, S.C. Taylor, Proc. Combust. Inst. 25 (1994) 749–757.
[28] L. Qiao, Y. Gu, W.J.A. Dahm, E.S. Oran, G.M. Faeth, Proc. Combust. Inst. 31 (2007) 2701–2709.
[29] L. Qiao, Y. Gu, W.J.A. Dahm, E.S. Oran, G.M. Faeth, Combust. Flame 151 (2007) 196–208.
[30] J.K. Bechtold, M. Matalon, Combust. Flame 67 (1987) 77–90.
[31] O.C. Kwon, G. Rozenchan, C.K. Law, Proc. Combust. Inst. 29 (2002) 1775–1784.
[32] C.K. Law, G. Jomaas, J.K. Bechtold, Proc. Combust. Inst. 30 (2004) 159–167.
[33] D. Bradley, M. Lawes, K. Liu, S. Verhelst, R. Woolley, Combust. Flame 149 (2007) 162–172.
[34] A.P. Kelley, C.K. Law, in: Fall Technical Meeting of the Eastern States Section of the Combustion Institute, 2007.
[35] Z. Chen, M.P. Burke, Y. Ju, Proc. Combust. Inst. (2009), doi:10.1016/j.proci.2008.05.060, in press.
[36] G.I. Sivashinksy, Astronaut. Acta 6 (1979) 631–645.
[37] A.S. Huzayyin, H.A. Moneib, M.S. Shehatta, A.M.A. Attia, Fuel 87 (2007) 39–57.
[38] J. de Vries, B.A. Corbin, E.L. Petersen, in: 5th US Combustion Meeting, March 25–28, 2007.
[39] C. Prathap, A. Ray, M.R. Ravi, Combust. Flame 155 (2008) 145–160.
[40] Z. Huang, Y. Zhang, K. Zenga, B. Liu, Q. Wang, D. Jiang, Combust. Flame 146 (2006) 302–311.
[41] J. Li, A. Kazakov, Z. Zhao, M. Chaos, F.L. Dryer, J.J. Scire Jr., Int. J. Chem. Kinet. 39 (2007) 109–136.
[42] J. Qian, G. Tryggvason, C.K. Law, J. Comput. Phys. 144 (1998) 52–69.
[43] B.T. Helenbrook, L. Martinelli, C.K. Law, J. Comput. Phys. 148 (1999) 366–396.
[44] W.S. Cleveland, J. Am. Stat. Assoc. 74 (1979) 829–836.
[45] J.R. Kee, F.M. Rupley, J.A. Miller, Sandia National Laboratories Report SAND 89-8009B, Livermore, CA, 1992.
[46] M.P. Burke, Y. Ju, F.L. Dryer, AIAA Paper AIAA-2008-1049, 2008.
[47] N. Lamoureux, N. Djebaili-Chaumeix, C.-E. Paillard, Exp. Therm. Fluid Sci. 27 (2003) 385–393.
[48] C. Tanga, Z. Huang, C. Jina, J. Hea, J. Wanga, X. Wanga, H. Miaoa, Int. J. Hydrogen Energy 33 (2008) 4906–4914.
[49] O.C. Kwon, G.M. Faeth, Combust. Flame 124 (2001) 590–610.
[50] C.K. Law, O.C. Kwon, Int. J. Hydrogen Energy 29 (2004) 867–879.
[51] H.Y. Sun, S.I. Yang, G. Jomaas, C.K. Law, Proc. Combust. Inst. 31 (2007) 439–446.
[52] J. Li, Z. Zhao, A. Kazakov, F.L. Dryer, Int. J. Chem. Kinet. 36 (2004) 566–575.
[53] S.G. Davis, A. Joshi, H. Wang, F.N. Egolfopoulos, Proc. Combust. Inst. 30 (2005) 1283–1292.